Hindawi
Journal of Nanomaterials
Volume 2019, Article ID 3481397, 11 pages
https://doi.org/10.1155/2019/3481397

Research Article

Hyaluronic Acid-Conjugated Mesoporous Silica Nanoparticles Loaded with Dual Anticancer Agents for Chemophotodynamic Cancer Therapy

Sanghyo Park,[1] Hyungkyu Park,[1] Seokhyeon Jeong,[1] Bong Gu Yi,[2] Kyeongsoon Park,[3] and Jaehong Key[1]

[1]*Department of Biomedical Engineering, Yonsei University, 1 Yonseidae-gil, Wonju, Gangwon-do 26493, Republic of Korea*
[2]*Interdisciplinary Graduate Program for BIT Medical Convergence and Department of Biology, College of Natural Sciences, Kangwon National University, Chuncheon, Gangwon-do 24341, Republic of Korea*
[3]*Department of Systems Biotechnology, Chung-Ang University, Anseong, Gyeonggi-do 17546, Republic of Korea*

Correspondence should be addressed to Kyeongsoon Park; kspark1223@cau.ac.kr and Jaehong Key; jkey@yonsei.ac.kr

Received 29 October 2018; Revised 8 January 2019; Accepted 20 January 2019; Published 4 April 2019

Academic Editor: Haisheng Qian

Present cancer treatments using chemotherapy are limited owing to both significant side effects to normal cells and high recurrence rates. In this study, we demonstrated cancer cell-targeting nanoparticles that load multiple anticancer agents for both specific treatments to cancer and substantial therapeutic effects. For this purpose, hyaluronic acid (HA) was conjugated to mesoporous silica nanoparticles (MSNs) for specifically targeting cancer cells. Moreover, the prepared HA-MSNs exhibited high drug loading potential and sustained drug release. Compared to bare MSNs, the HA-MSNs were internalized at an approximately three times higher rate in squamous cell carcinoma 7 (SCC7) cells. To enhance the anticancer effects of chemotherapy and photodynamic therapy (PDT), doxorubicin (DOX) and chlorin e6 (Ce6) were loaded in HA-MSNs (DOX/Ce6/HA-MSNs); the product exhibited highly effective cytotoxicity on green fluorescent protein-expressing squamous cell carcinoma 7 (SCC7) compared to the corresponding free drugs and HA-MSNs with DOX or Ce6 alone. This study indicates that the application of DOX/Ce6/HA-MSNs in chemotherapy and PDT exerts significant therapeutic effects against SCC7.

1. Introduction

Over the past 50 years, a large number of nanoparticles have been reported for improving therapeutic effects in tumor treatment [1]. The main purpose of the development of nanoparticles is to achieve effective drug delivery systems and maximize therapeutic effects [2, 3]. Among the various nanoparticles, mesoporous silica nanoparticles (MSNs) can be used as a drug delivery system loaded with multiple drugs to improve the therapeutic effects compared to the corresponding free drugs [4–6]. MSNs as drug delivery systems have also produced results exhibiting potential for chemotherapy and photodynamic therapy (PDT) [7, 8]. MSNs can incorporate hydrophobic anticancer drugs [9, 10]. The sequestration of drug molecules within the hydrophobic cores of MSNs enables sustained drug release properties in a regulated manner. MSNs can be conveniently modified for external triggering by pH, temperature, ultrasound, and light [11].

To improve the drug delivery efficiency, specific targeting ligands such as peptides and antibodies have been tethered to the surface of nanoparticles via surface charge interaction or chemical conjugation [12]. Targeted nanoparticles more efficiently eradicate tumor tissues and provide increased cellular uptake compared to untargeted particles. For example, hyaluronic acid- (HA-) based nanoparticles are of high interest in targeted drug delivery systems and imaging probes. At present, the opportunity to develop a novel drug carrier with HA shown its novelty in tumor cell-specific targeting [13]. HA can be utilized as a specific ligand for targeting CD44- and CD168-overexpressing tumor cells such as Hela cells, HT29 cells, and SCC7 cells [14–17].

Monotherapy approaches using drugs such as dabrafenib and selumetinib represent conventional treatment methods for numerous types of tumors. However, monotherapeutic techniques result in the decimation of both healthy and cancerous cells owing to their nonspecific targeting, yielding insufficient therapeutic effects [18]. Combinatorial therapies, where two or more therapeutics are simultaneously used, generally result in enhanced therapeutic efficacy via additive or synergistic effects and can overcome drug resistance mechanisms. Moreover, the combinatorial approach can decrease the toxic effects on healthy cells owing to the lower therapeutic dosage of each administered drug while simultaneously enhancing the cytotoxic effects on cancer cells [19, 20]. However, conventional cocktail-based combinatorial therapy is generally limited by inconsistent tissue distribution and different cell permeability of individual drugs [21]. Encapsulating multiple drugs in nanosized drug carriers can achieve consistent pharmacokinetics and higher therapeutic effects; this depends on the physicochemical properties of the drug carriers such as the particle size, immune reaction, and surface charge [22–25].

PDT is a local treatment for oncological, cardiovascular, dermatological, and ophthalmic diseases [26–31]. PDT uses singlet oxygen (SO, $^1O_2$) produced from photosensitizer (PS) molecules under suitable light irradiation to induce cytotoxicity. Compared to chemotherapy or radiotherapy, PDT exhibits relatively minimal side effects when used in tumor treatments [32]. Recent studies have indicated that the combination of chemotherapy and PDT improves anticancer efficacy. Combination therapies that combine more than two treatments, such as chemotherapy and PDT, prevent drug resistance and produce synergistic anticancer effects; thereby, they inhibit P-glycoprotein-mediated drug efflux, which is a major drug resistance mechanism [33–36].

In this study, we developed HA-conjugated MSNs incorporating DOX and Ce6 (DOX/Ce6/HA-MSNs) for targeted chemotherapy and PDT to treat squamous cell carcinoma 7 (SCC7); this approach maximized the synergistic effects of the components. We compared the therapeutic effects of free DOX, free Ce6, DOX-loaded HA-MSNs (DOX/HA-MSNs), Ce6-loaded HA-MSNs (Ce6/HA-MSNs), and DOX and Ce6-loaded HA-MSNs (DOX/Ce6/HA-MSNs). In this comparison, we demonstrated that DOX/Ce6/HA-MSNs exhibited the result exhibiting the highest potential for removing SCC7 cells.

2. Experiment

2.1. Materials. Cetyltrimethylammonium bromide (CTAB, 98%), tetraethyl orthosilicate (TEOS, 99%), methylene (98%), and (3-aminopropyl)triethoxysilane (APTES, 99%) were purchased from Sigma-Aldrich Co. (Milwaukee, WI). Hyaluronic acid (HA; MW 6,400 and 215,000 Da) was purchased from Lifecore Biomedical (Chaska, MN, USA). 4-(4,6-Dimethoxy-1,3,5-triazin-2-yl)-4-methylmorpholinium chloride n-hydrate (DMT-MM) was purchased from Wako Pure Chemical Industries Ltd. (Tokyo, Japan). Doxorubicin (DOX), dimethyl sulfoxide (DMSO), 1-ethyl-3-(3-dimethylaminopropyl)carbodiimide (EDC), and *N*-hydroxysuccinimide (NHS) were purchased from Sigma-Aldrich Co. (MO, USA). Chlorin e6 (Ce6) was purchased from Santa Cruz Biotechnology (Texas, USA). Singlet oxygen sensor green® (SOSG) reagent was purchased from Molecular Probes (Eugene, Oregon, USA). For cell culture, RPMI-1640 (Gibco BRL, Rockville, MD, USA) supplemented with 10% (*v*/*v*) fetal bovine serum (FBS) and 1% antibiotic-antimycotic solution was used. RPMI-1640, FBS, and phosphate-buffered saline (PBS) were purchased from Lonza Walkersville (Basel, Switzerland). 10% (*v*/*v*) fetal bovine serum (FBS) was purchased from GenDEPOT Inc. (Texas, USA). The cell counting kit-8 (CCK-8) was purchased from Dojindo Laboratories Co. Ltd. (Kumamoto, Japan). All the reagents used were of analytical grade.

2.2. Synthesis and Surface Functionalization of MSNs. The MSNs were synthesized according to a previous report [37]. Briefly, mesitylene (10.5 mL, 73.2 mM) was added to an aqueous solution of CTAB (1.5 g, 4.1 mM) and mixed with 2-M NaOH (3.5 mL). After settling at 80°C, TEOS (7.5 mL, 33 mM) was added dropwise at the rate of 1 mL/min, and the mixture was stirred vigorously. After 2 h, the mixture was precipitated in methanol; the precipitates were isolated by filtration, washed with methanol, and dried at 65°C for one day to remove methanol. The crude MSN (2 g) was suspended in a methanolic solution (200 mL) containing concentrated HCl (1.5 mL) under sonication for 10 min and stirred for 6 h at 50°C to remove unreacted CTAB and mesitylene. Subsequently, the MSNs were isolated via filtration, washed with methanol, and dried at 65°C for one day. To obtain amine-functionalized MSNs (MSN-NH_2), the dried MSNs (500 mg) were refluxed in a toluene (10 mL) solution containing APTES (5 mL) at 110°C for 15 h. After this reaction, the MSN-NH_2 was isolated via filtration, washed with n-hexane and ethanol, and dried at 65°C for one day.

To target CD44 receptors expressed on the cancer cell surfaces, HA was chemically coupled to the surface of the MSN-NH_2. HA (100 mg, MW 6,400) dissolved in deionized water (DW, 25 mL) was reacted with DMT-MM (43.2 mg) for 30 min to activate the carboxylic groups of HA. The activated HA was reacted with MSN-NH_2 (1 g) well-dispersed in DW (20 mL) for 12 h. Subsequently, the HA-modified MSNs (HA-MSNs) were centrifuged, washed three times with distilled water, and lyophilized for 2 days. To further evaluate the surface modification of HA on MSN-NH_2 and the intracellular uptake of HA-MSNs, the prepared Cy5.5-labeled HA (20 mg) (prepared via chemical conjugation of Cy5.5-NH_2 (5 mg) and HA (100 mg, MW 6,400) in the presence of DMT-MM (15 mg)) was chemically coupled to MSN-NH_2 (200 mg) using DMT-MM (8.6 mg) as described above. Fluorescence imaging of HA-MSNs dispersed in DW was performed using an IVIS imaging system (IVIS 200, Xenogen Corporation, CA, USA).

2.3. Characterization of the Surface-Functionalized MSNs. To characterize the particle size, shape, and porosity, a variable pressure field emission scanning electron microscope (VP-FE-SEM; SUPRA-55VP, Carl Zeiss, Germany) and energy-filtered transmission electron microscope (EF-TEM;

LEO912AB, Carl Zeiss) were used. For TEM analysis, a drop of the sample solution in methanol (0.5 mg/mL) was placed on a 200-mesh copper grid coated with carbon and air-dried prior to measurement. To verify the modification of the HA on the surface of the MSNs, solid-state ^{13}C cross-polarization magic angle spinning (CP/MAS) nuclear magnetic resonance (NMR) measurements were recorded at 400 MHz using a Bruker Avance II+ nuclear magnetic resonance spectrometer (Germany); this spectrometer had with a 4.0 mm zirconia rotor CP/MAS probe and a sample spinning rate of 8 kHz. The CP/MAS spectra were acquired with a delay time of 3.0 s.

Nitrogen adsorption-desorption analysis was performed using an adsorption analyzer (Micromeritics ASAP 2020, USA). According to the adsorption data, the Brunauer–Emmett–Teller (BET) and Barrett–Joyner–Halenda (BJH) models were used to calculate the specific surface area and pore size, respectively, of the prepared MSNs. The particle size distribution and zeta potential of the MSNs (1 mg) in 150 nM PBS (1 mL, pH 7.4) were measured using a Zetasizer 3000 instrument (Malvern Instruments Ltd.). To further evaluate the *in vitro* stability of the prepared HA-MSNs, 1 mg of the HA-MSNs was dispersed in PBS (pH 5.5 or 7.4), and the particle sizes were monitored for four days using a Zetasizer Nano-zs90 (Malvern Instruments Ltd., Malvern, UK).

2.4. Characterization of the Drug-Loaded HA-MSNs. The dried HA-MSNs (0.9 mg) were dispersed in PBS (0.9 mL) and sonicated using a probe-type sonicator for 10 min. Ce6 (0.5 mg) was dissolved in 0.5 mL of ethanol, and DOX (0.5 mg) was dissolved in DMSO (0.5 mL). The Ce6 and DOX solutions were added dropwise to the HA-MSN solution (1 mg/mL) and stirred under light-protected conditions for 24 h. After centrifuging the resulting solution at 13,500 rpm for 15 min, the supernatant was collected to determine the drug loading content and efficiency. Subsequently, the drug-loaded HA-MSNs were washed three times with PBS and redispersed in PBS (1 mL). The particle sizes and zeta potential values of the drug-loaded HA-MSNs were measured using a Zetasizer Nano-zs90.

To determine the drug loading content and efficiency, the residual amount of drugs (Ce6 or DOX) in the collected supernatant was measured using a Synergy HTX multimode plate reader at 404 nm for Ce6 and 485 nm for DOX. Standard curves of the drugs (Ce6 or DOX) were used to calculate the remaining drug loading content and efficiency. The drug loading content was expressed as the mass of the drugs (Ce6 or DOX) loaded per gram of HA-MSNs, using the following formula [38]:

$$\text{Encapsulation efficiency}(\%) = \frac{[\text{Drug}]_i - [\text{Drug}]_s}{[\text{Drug}]_i} \times 100. \quad (1)$$

2.5. In Vitro Drug Release Study. To analyze the amount of $[\text{Drug}]_i$ drug released from the drug-loaded HA-MSNs (DOX/HA-MSNs, Ce6/HA-MSNs, and DOX/Ce6/HA-MSNs), each sample (1 mg) was dispersed and placed in a dialysis membrane (MWCO; 10 kDa) immersed in PBS (pH 7.4); this was followed by gentle shaking in a water bath at 37°C, oscillating 100 times/min. Fresh medium was added at predetermined intervals. To measure the amount of drug released, the absorbance was recorded at 404 nm for Ce6 and 485 nm for DOX. A calibration curve of the released drug was constructed using drug solutions of specified concentrations according to the Lambert–Beer law [39].

2.6. Singlet Oxygen (SO) Generation Study. The SO generation induced by Ce6, Ce6/HA-MSNs, and DOX/Ce6/HA-MSNs was evaluated by measuring the fluorescence-intensity of the SOSG during light irradiation. Ce6/HA-MSNs (equivalent of 5 μM Ce6) and DOX/Ce6/HA-MSNs (equivalent of 5 μM Ce6 and 5.1 μM DOX) were dispersed in oxygen-saturated PBS. For comparison, free Ce6 (equivalent of 5 μM Ce6), Ce6/HA-MSNs (equivalent of 5 μM Ce6), and DOX/Ce6/HA-MSNs (equivalent of 5 μM Ce6 and 5.1 μM DOX) were dissolved in oxygen-saturated PBS containing Tween 20 (1%, *v*/*v*). All the groups also contained 1 μM of SOSG (Ex/Em: 504/525 nm). The SOSG fluorescence intensity was measured at 525 nm after the light irradiation via continuous wave (CW) laser (irradiation dose: 50 mW/cm^2) at 670 nm.

2.7. Cell Culture, Intracellular Uptake, and Blocking Experiments. Green fluorescent protein-expressing squamous cell carcinoma 7 (SCC7) cells were maintained in RPMI-1640 supplemented with 1% penicillin and 10% FBS in a humidified incubator with 5% CO_2 at 37°C. The medium was regularly changed every two days.

To test the *in vitro* cellular uptake of HA-MSNs against SCC7 cells, SCC7 cells (5×10^4 cells/mL/well) were seeded in a confocal dish and permitted to adhere for 24 h. The medium was replaced with a serum-free medium (2 mL) containing Cy5.5-labeled HA-MSNs (0–100 μg/mL). To verify the internalization of the drug-loaded nanoparticles, the medium was replaced with a serum-free medium (2 mL) containing DOX/HA-MSNs (equivalent of 5.1 μM DOX), Ce6/HA-MSNs (equivalent of 5 μM Ce6), or DOX/Ce6/HA-MSNs (equivalent of 5 μM Ce6 and 5.1 μM DOX), and the cells were incubated for an additional 24 h.

For the blocking experiments, the cells (5×10^4 cells/mL/well) were seeded in a confocal dish and permitted to adhere for 24 h. Then, the medium was replaced with a serum-free medium (2 mL) containing HA (10 mg, MW = 6,400); this was followed by an additional 2 h of incubation. After the addition of DOX/HA-MSNs (equivalent of 5.1 μM DOX), Ce6/HA-MSNs (equivalent of 5 μM Ce6), or DOX/Ce6/HA-MSNs (equivalent of 5 μM Ce6 and 5.1 μM DOX), the cells were incubated for an additional 2 h.

After the cells were treated, they were washed with PBS (pH 7.4), fixed with a 4% paraformaldehyde solution for 30 min, and washed two times with PBS (pH 7.4). Subsequently, the cells were incubated in a DAPI solution (2 mL, 500 nM) over 30 min at 37°C. After the incubation, the cells were washed two times with PBS (pH 7.4). The intracellular

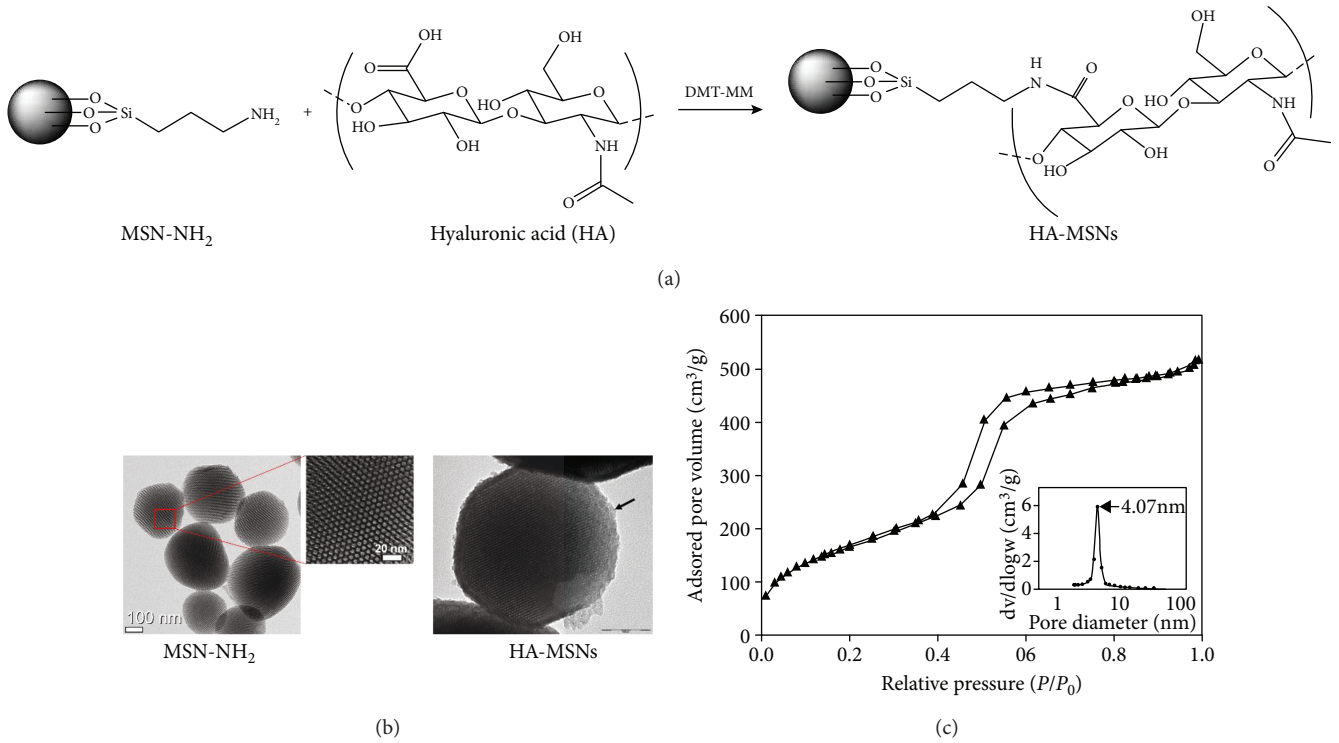

Figure 1: (a) Synthesis of HA-MSNs. (b) Morphology of MSN-NH_2 and HA-MSNs observed by TEM. (c) N_2 adsorption-desorption isotherms of MSN-NH_2.

uptake and blocking experiments were observed using a confocal scanning microscope (ZEISS LSM 710, Germany). In addition, to compare the intracellular uptakes of the DOX/-HA-MSNs (equivalent of 5.1 μM DOX), Ce6/HA-MSNs (equivalent of 5 μM Ce6), and DOX/Ce6/HA-MSNs (equivalent of 5 μM Ce6 and 5.1 μM DOX) in the SCC7 cells after the blocking experiments, the fluorescence intensity of the cells in each group was determined.

2.8. In Vitro Cytotoxicity and Phototoxicity of the SCC7 Cells. The *in vitro* cytotoxicity of each sample was evaluated on the SCC7 cells using a CCK-8 assay kit. The SCC7 cells (5×10^3 cells/well) were seeded in 96-well plates and permitted to adhere for 24 h. The cells were treated with DOX, Ce6/HA-MSNs, DOX/HA-MSNs, or DOX/Ce6/HA-MSNs of different concentrations (equivalent of 0.31, 0.63, 1.25, 2.5, and 5 μM Ce6; equivalent of 0.32, 0.64, 1.28, 2.6, and 5.1 μM DOX) under light-protected conditions for 24 h. Subsequently, the cells were washed with culture medium, and a CCK-8 assay solution was added to the cells. According to the manufacturer's instructions, the cells were further incubated for 1 h at 37°C. The cytotoxicity was evaluated by measuring the optical density using a Synergy HTX multimode plate reader at 450 nm.

To investigate the *in vitro* phototoxicity of free Ce6, Ce6/HA-MSNs, and DOX/Ce6/HA-MSNs, the cells were prepared via the methods used in the dark toxicity test. The medium was changed with a serum-free medium containing either free Ce6 (equivalent of 5 μM Ce6), Ce6/HA-MSNs (equivalent of 5 μM Ce6), or DOX/Ce6/HA-MSNs (equivalent of 5 μM Ce6 and 5.1 μM DOX). After incubation for 30 min, the medium was changed, and the cells were irradiated with a 670 nm CW laser (50 mW/cm^2) for 1 or 2 min; this was followed by incubation of the cells for an additional 18 h. The phototoxic effects of free Ce6, Ce6/HA-MSNs, or DOX/Ce6/HA-MSNs on the SCC7 cells were analyzed using the CCK-8 assay kit as described above. The optical density was measured using a Synergy HTX multimode plate reader at 450 nm. For the control experiment, the cells without radiation were evaluated simultaneously.

2.9. Statistical Analysis. The data were expressed as mean ± standard deviation, and the comparisons were performed using one-way ANOVA tests (Systat Software Inc., Chicago, IL, USA). The differences were considered statistically significantly at $^*p < 0.05$, $^{**}p < 0.01$, $^{***}p < 0.005$, and $^{****}p < 0.001$.

3. Results and Discussion

The MSNs were reacted with APTES to introduce terminal amino groups and afford MSN-NH_2 [40, 41]. The SEM and TEM images reveal that the MSN-NH_2 exhibited a diameter ranging from 250 to 500 nm with a well-ordered hexagonal mesoporous structure (Figure 1(b)). A thin layer, indicated by an arrow, was observed on the surface of the HA-MSNs; this demonstrates that HA molecules were immobilized on the MSN-NH_2 surface. The nitrogen adsorption-desorption plot of the MSN-NH_2 exhibits a typical type-IV isotherm profile, indicating the presence of mesopores [41]. The BET surface area, BJH desorption pore volume, and average pore diameter were calculated to be 621.5 m^2/g, 0.831 cm^3/g, and

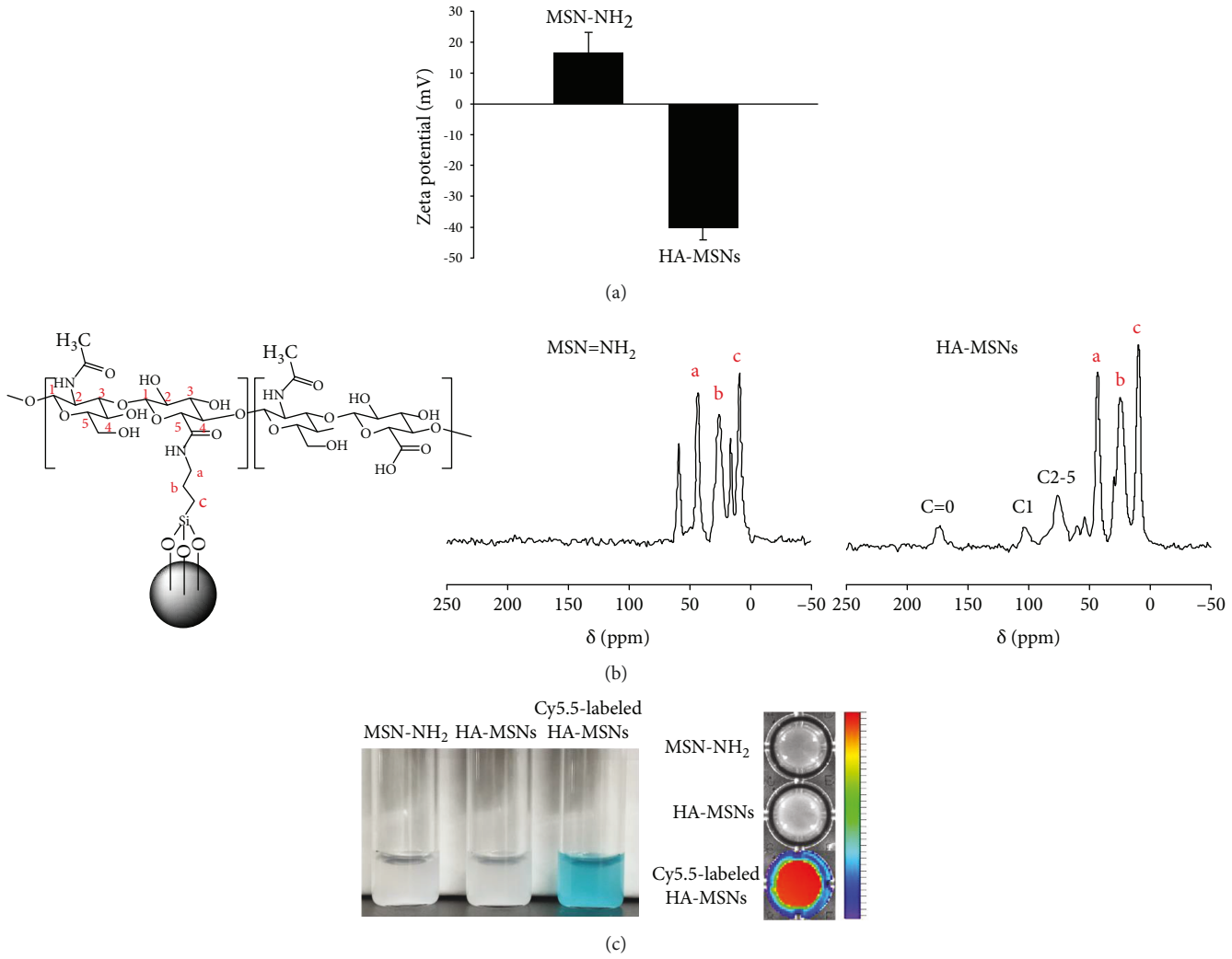

Figure 2: (a) Zeta potential of the MSN-NH_2 and HA-MSNs. (b) ^{13}C NMR spectra of the MSN-NH_2 and HA-MSNs. (c) Photo and fluorescence image of the MSN-NH_2, HA-MSNs, and Cy5.5-labeled HA-MSNs.

4.07 nm, respectively; these are suitable for drug loading (Figure 1(c)).

To graft the HA molecules via an amide linkage, the amine groups of MSN-NH_2 were chemically reacted with the carboxylic groups of HA in the presence of DMT-MM as a crosslinker (Figure 1(a)). The zeta potential of the MSN-NH_2 was 16.4 ± 6.79 mV owing to the amine groups on the silica surface [41]. After conjugating HA, the zeta potential of the HA-MSNs changed to a negative value (-40.0 ± 4.10 mV) (Figure 2(a)); this is attributable to the carboxylic groups of HA molecules. The HA-grafting on the surface of the MSN-NH_2 was also verified by ^{13}C solid NMR analysis (Figure 2(b)). The peaks observed at approximately 43, 26, and 9 ppm in the MSN-NH_2 spectrum can be assigned to the three types of methylene carbons on the APTES immobilized on the MSNs. These three peaks were also observed in the spectrum of the HA-MSNs; the other peaks at 66–184 ppm can be attributed to the C1 anomeric carbons, C2–C5 carbons, and carboxylate and/or carbonyl acetamide carbons of the HA polymers (103, 76, and 173 ppm, respectively; see the HA structure and indexing)

Table 1: Drug loading efficiency and content of Ce6 or DOX in the DOX/HA-MSNs, Ce6/HA-MSNs, and DOX/Ce6/MSNs.

Samples	Loading efficiency (%)	Loading content (%)
DOX/HA-MSNs	91.46 (DOX)	9.22 (DOX)
Ce6/HA-MSNs	86.93 (Ce6)	8.81 (Ce6)
DOX/Ce6/HA-MSNs	46.10 (DOX)	5.17 (DOX)
DOX/Ce6/HA-MSNs	48.32 (Ce6)	5.10 (Ce6)

[41, 42]. To verify the HA grafting on the MSN-NH_2, Cy5.5-labeled HA-MSNs were synthesized. The MSN-NH_2 and HA-MSNs without Cy5.5 exhibited no color or fluorescence signals, whereas the Cy5.5-labeled HA-MSNs were sky blue and exhibited a strong fluorescence signal (Figure 2(c)). These results indicated that HA was successfully grafted on the surface of the MSN-NH_2.

The drug loading efficiency and content of Ce6/HA-MSNs, DOX/HA-MSNs, and DOX/Ce6/HA-MSNs

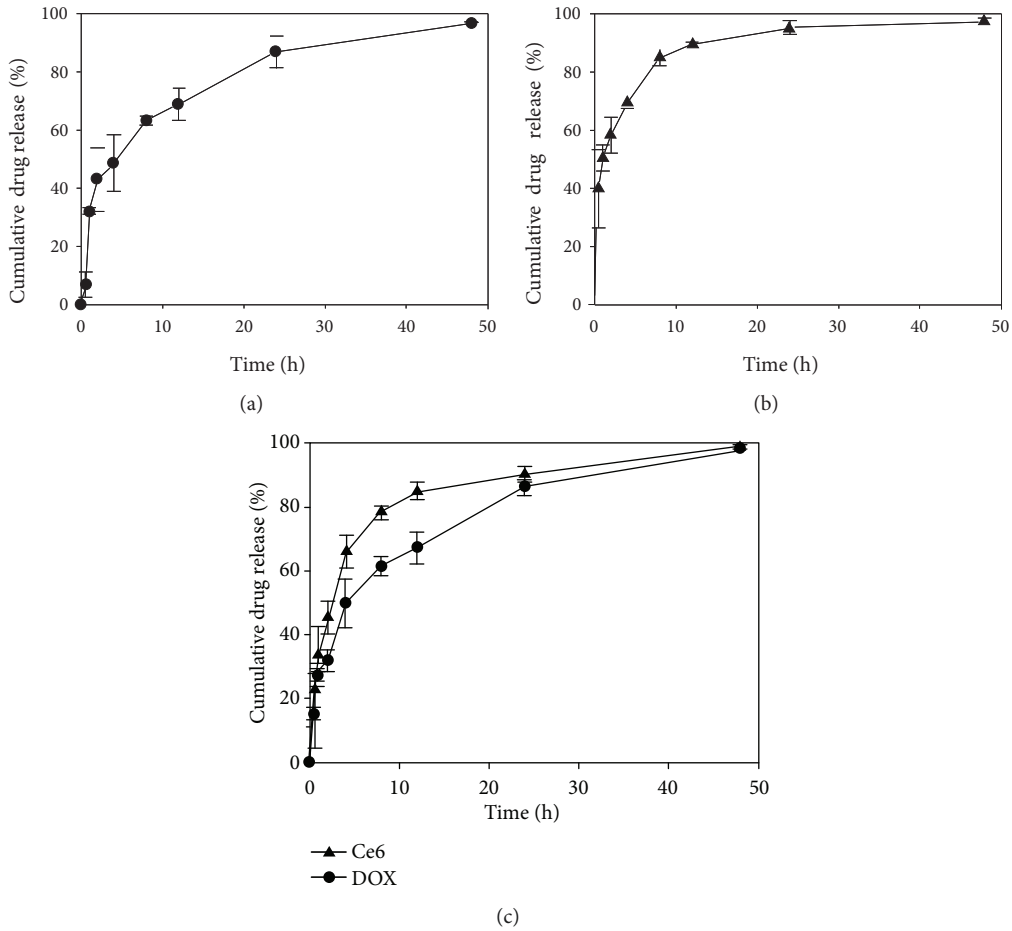

Figure 3: Release profiles of Ce6 or DOX from (a) Ce6/HA-MSNs, (b) DOX/HA-MSNs, and (c) DOX/Ce6/HA-MSNs.

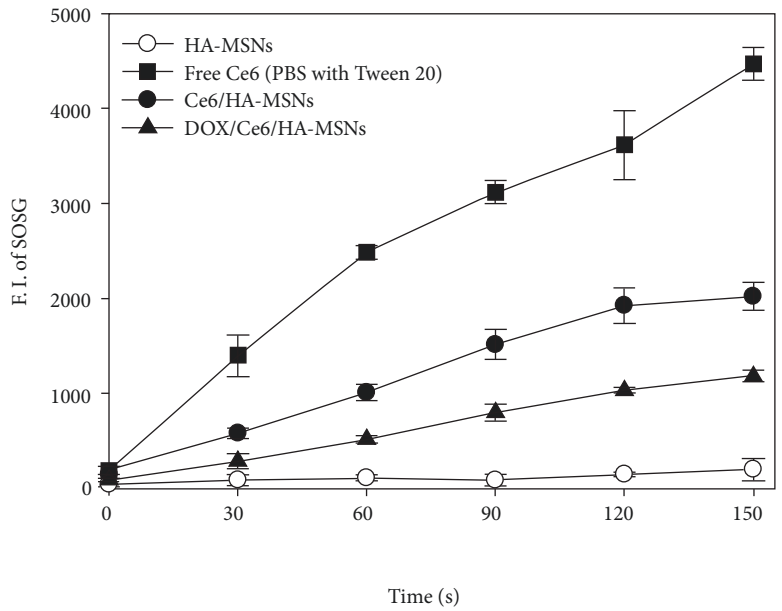

Figure 4: Changes in SOSG fluorescence intensity at 525 nm as a function of laser irradiation time.

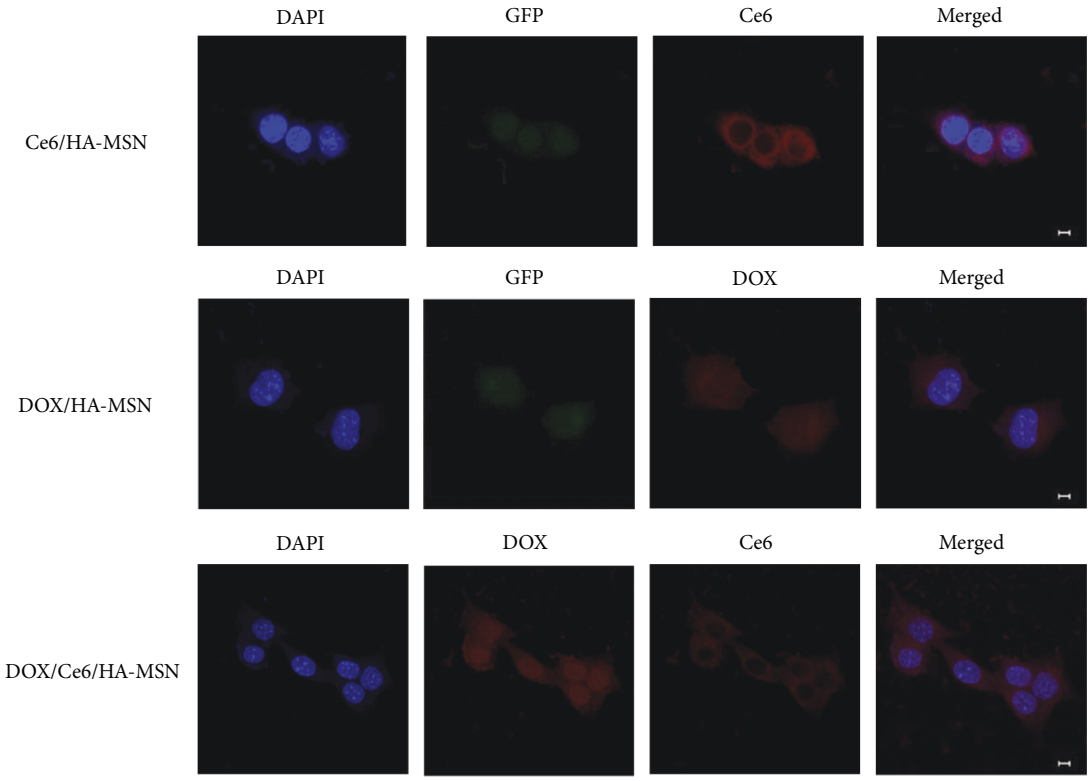

Figure 5: Intracellular uptakes of Ce6/HA-MSNs, DOX/HA-MSNs, and DOX/Ce6/HA-MSNs against SCC7 (scale bar: 5 μm).

were determined by UV-vis absorption (Table 1). Owing to their typical absorbance peaks in DOX and Ce6, an error that can be caused by the absorbance band overlap between DOX and Ce6 would not be significant to affect the result of the calculation of drug loading capacity [43]. The loading of drugs in the HA-MSNs was 9.15% for Ce6/HA-MSNs, 9.48% for DOX/HA-MSNs, or 5.14% (Ce6) and 5.19% (DOX) for DOX/Ce6/HA-MSNs. Owing to the hydrophobic properties of Ce6 and DOX, these drugs were loaded within the hydrophobic pores of the HA-MSNs with a high loading efficiency.

It appears that the well-developed homogeneous surface pores arrayed on the surface of the particle can contain an adequate number of anticancer drug molecules such as DOX and Ce6. This result demonstrates that Ce6 and DOX were loaded adequately to the surface of the pores through the observed change in the color of the sample from white to reddish [44].

In addition, the cumulative drug release curves of Ce6/HA-MSNs, DOX/HA-MSNs, and DOX/Ce6/HA-MSNs in PBS at 37°C are shown in Figure 3. Conceptually, this result shows DOX and Ce6 were in the surface of pores in HA-MSNs being released in time.

During the first 8 h, a rapid release of Ce6 or DOX was observed in all the systems. Subsequently, a gradual drug release was observed up to the cumulative release time of 48 h. For Ce6/HA-MSNs and DOX/HA-MSNs, the Ce6 and DOX release reached 84% and 95%, respectively, at 24 h. For DOX/Ce6/HA-MSNs, the Ce6 and DOX were released at rates of 84% and 90%, respectively, after 24 h. This indicated that the nanoparticle systems exhibited similar cumulative drug release trends at 24 h, with no remarkable differentiation. Meanwhile, the release profiles are likely to have been affected by the different pH conditions. Whereas a previous study reported that the rate of release of DOX from MSNs was similar at both pH 5.0 and pH 7.4 [45], another study indicated that low stability and hydrolysis of MSNs in an acidic condition can cause faster drug release than those in a neutral or an alkaline condition [46]. Thus, further investigation is required to verify it.

For effective PDT, the generation of singlet oxygen (SO) from the photoactivatable agents was evaluated. The SO generation from the Ce6/HA-MSNs and DOX/Ce6/HA-MSNs after light irradiation was monitored chemically with SOSG as a highly selective reagent for $^1O_2$ [47] (Figure 4). SOSG is weakly fluorescent without SO, whereas it emitted a strongly fluorescent signal after reaction with $^1O_2$ [48]. During 670 nm laser irradiation, a marginal increase in the SOSG fluorescence emission was observed for Ce6/HA-MSNs and DOX/Ce6/HA-MSNs compared to that for free Ce6 in the solubilized state. This indicated that the SO generation was inhibited in the quenched state of Ce6/HA-MSNs and DOX/Ce6/HA-MSNs and that the hydrophobic Ce6 molecules were successfully loaded within the HA-MSNs. As shown in Figure 4, the SOSG fluorescence of free Ce6 was the highest. The likely explanation is that the Ce6 molecules encapsulated in the MSNs were continuously released and were not completely exposed during the laser irradiation.

To evaluate the cytotoxicity and the CD44 receptor-mediated endocytosis of the nanoparticles, SCC7 cells were incubated with the prepared HA-MSNs. Most of

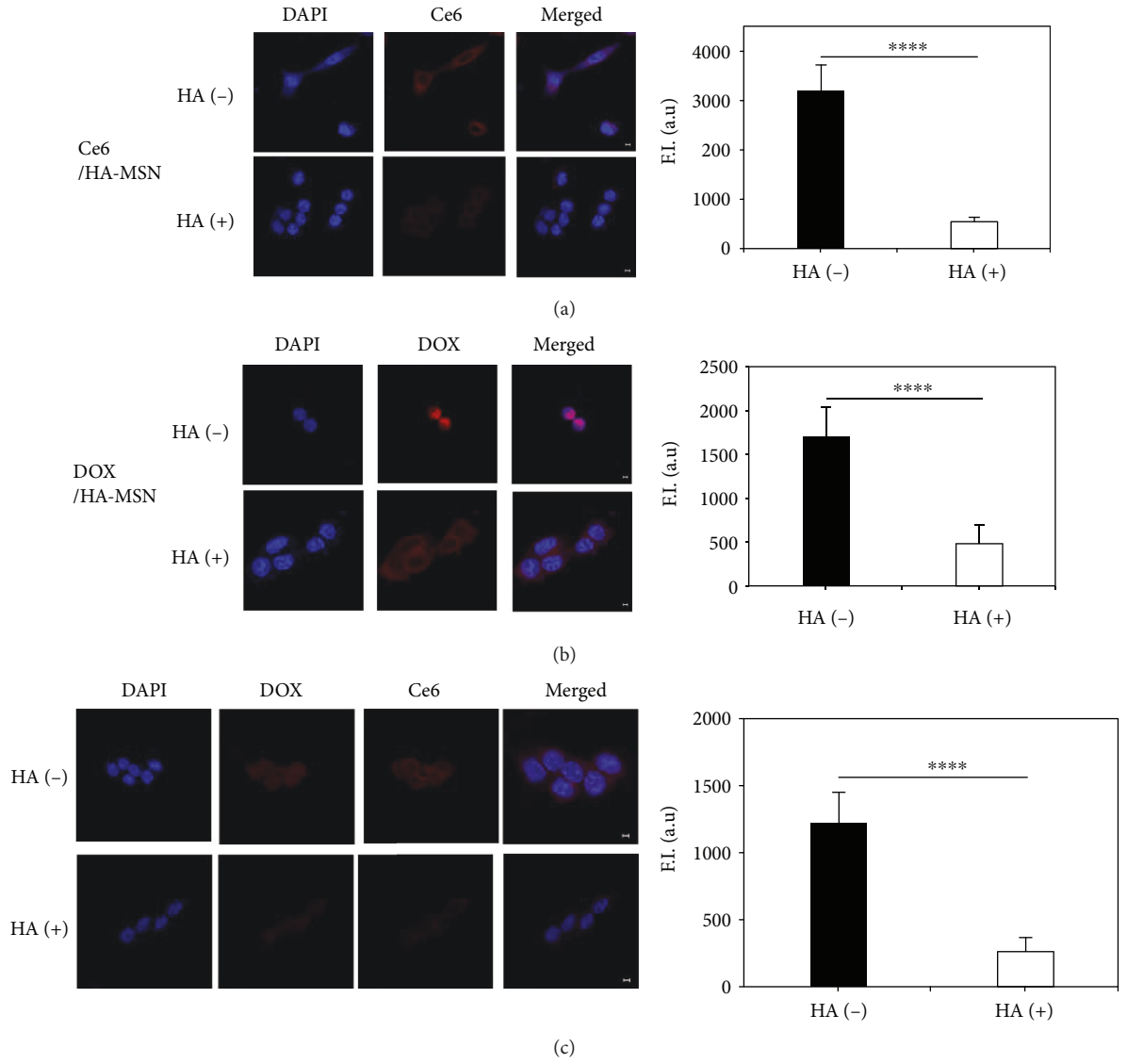

Figure 6: Comparison of intracellular uptake and quantitative average fluorescence intensities of (a) Ce6/HA-MSNs, (b) DOX/HA-MSNs, and (c) DOX/Ce6/HA-MSNs in SCC7 cells treated with or without free HA (scale bar: 5 μm, $^{****}p < 0.001$).

the cells (>95%) were viable up to 250 μg/mL of HA-MSNs; this indicates that HA-MSNs are nontoxic and biocompatible nanocarriers (Supporting Information, Figure S1).

The intracellular uptake and CD44-mediated endocytosis of HA-MSNs with or without drugs were examined against SCC7 cells, which express CD44 receptors [15]. After 1 h of incubation with Cy5.5-labeled HA-MSNs, the fluorescence intensity increased significantly in a concentration-dependent manner (Supporting Information, Figure S2).

DOX is localized in a nucleus that is stained in blue by DAPI (Supporting Information, Figure S3). Moreover, the localization of DOX in tumor cells could be a function of the incubation time, and it can remain in the cytosol if the cells had been captured while passing from the cytosol to the nucleus. It was observed that DOX was localized in the cytosol while shifting from the outer section to the nucleus through endocytosis [49].

Otherwise, Ce6 is localized in the cytosol of tumor cells; SCC7 is mainly outside the membrane of the nucleus. The nucleus is stained in blue by DAPI. There is no overlapped location between Ce6 and the nucleus (Supporting Information, Figure S4).

The fluorescence images shown in Figure 5 demonstrate that all the cells treated with the Ce6/HA-MSNs, DOX/-HA-MSNs, and DOX/Ce6/HA-MSNs exhibited red fluorescence dispersed in the cytoplasm or nuclei; this implies that the three drug-loaded HA-MSNs were successfully internalized by the SCC7 cells. The fluorescence of Ce6 was mainly observed in the cytoplasm of the cells treated with Ce6/HA-MSNs; meanwhile, the DOX fluorescence signal was observed primarily in the nuclear region, indicating that the DOX permeated the nuclear envelope and intercalated DNA [50]. Furthermore, when the cells were incubated with free HA as a specific CD44 ligand following the treatment of Ce6/HA-MSNs, DOX/HA-MSNs, or

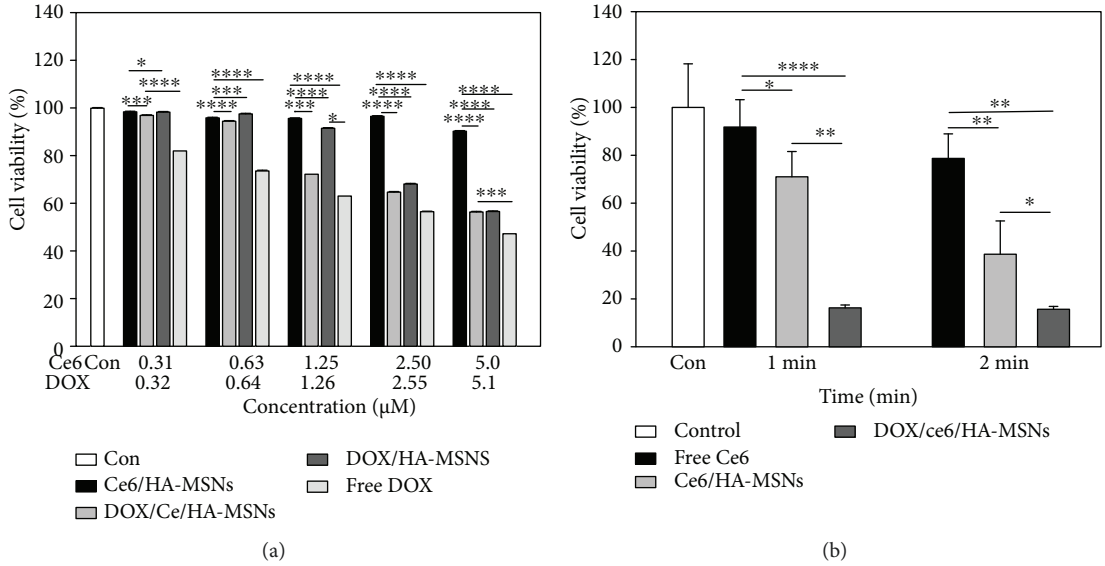

Figure 7: (a) Dark cytotoxicity of Ce6/HA-MSNs, DOX/HA-MSNs, DOX/Ce6/HA-MSNs, or free DOX on SCC7 cells. (b) Phototoxicity of Ce6/HA-MSNs, DOX/Ce6/HA-MSNs, or free Ce6 on SCC7 cells irradiated with a 670 nm wavelength laser (50 mW/cm^2; $^*p < 0.05$, $^{**}p < 0.01$, $^{***}p < 0.005$, and $^{****}p < 0.001$).

DOX/Ce6/HA-MSNs, the fluorescence intensities in the cells decreased significantly (Figure 6). This indicated that the free HA bound to the CD44 receptor is likely to have blocked the bond between the CD44 receptor and HA-MSNs loaded with Ce6 and/or DOX [51]. The intracellular uptake of nanoparticles indicates that Ce6/HA-MSNs, DOX/HA-MSNs, and DOX/Ce6/HA-MSNs can specifically target SCC7 cells (high expression of the CD44 receptor) and that their intracellular uptakes were achieved via receptor-mediated endocytosis.

DOX/HA-MSNs and DOX/Ce6/HA-MSNs were examined against SCC7 cells. The SCC7 cells treated with free DOX, DOX/HA-MSNs, and DOX/Ce6/HA-MSNs exhibit DOX dosage-dependent cytotoxic effects (Figure 7(a)). Free DOX significantly decreased the cell viability in a dose-dependent manner. Although the DOX/MSNs and DOX/Ce6/HA-MSNs also exhibited cytotoxic effects, the cells treated with DOX/MSNs and DOX/Ce6/HA-MSNs exhibited higher cell viabilities than those exposed to free Dox. The cytotoxic effect of the DOX/MSNs and DOX/Ce6/-HA-MSNs could be induced after the DOX release from the nanoparticles, resulting in reduced cytotoxicity compared to the free DOX at identical time points. Meanwhile, the cells treated with Ce6/HA-MSNs exhibited >90% cell viability, indicating that the Ce6/HA-MSNs exerted no cytotoxic effects on the SCC7 cells without irradiation.

The *in vitro* chemo- and PDT effects of the free Ce6, Ce6/HA-MSNs, and DOX/Ce6/HA-MSNs on SCC7 cells were investigated using a CCK-8 kit. The cell viability was normalized to the control cells (no drug or laser irradiation). The treatments with free Ce6, Ce6/HA-MSNs, or DOX/Ce6/-HA-MSNs on the SCC7 cells were followed by studies on the laser irradiation-induced concentration-dependent phototoxicity (Figure 7(b)). The PDT effect of the Ce6/HA-MSNs is approximately two times higher than that of the free Ce6 alone after 2 min of irradiation. Ce6 (5 μM) provoked approximately 25% cell death after 2 min of laser irradiation, whereas approximately 63% cell death was observed in the Ce6/HA-MSN-treated cells. The treatment of the DOX/-Ce6/HA-MSNs followed by laser irradiation induced the cell death of approximately 80% after 1 min of laser irradiation. These results demonstrate that DOX/Ce6/HA-MSNs exhibit better therapeutic effects on CD44 receptor-expressing cancer cells than monodrug-loaded-HA-MSNs.

Based on the *in vitro* results, we have recognized that the availability after it has been administrated and circulated *in vivo* should be identified and tested to determine the appropriate usage of the DOX/Ce6/HA-MSNs in different therapeutic working environments such as chemotherapy and photodynamic therapy and the method for circulating *in vivo* after the administration. It is likely to be a highly effective approach toward optimal cancer treatment in the future.

4. Conclusions

In this study, we designed CD44-targetable MSNs for chemo- and PDT cancer therapy to alleviate the side effects of chemotherapy and synergistically induce therapeutic effects. We demonstrated that HA-MSNs are favorable nanocarriers with a remarkable CD44-targeting capability for effective dual-drug (DOX and Ce6) delivery to CD44-expressing cancer cells. DOX/Ce6/HA-MSNs exhibited cytotoxic effects after intracellular delivery of Dox *via* CD44-mediated endocytosis and remarkable phototoxicity induced by highly reactive SO generation in SCC7 cells after laser irradiation. These results indicate that chemo- and photoactivatable DOX/Ce6/HA-MSNs exhibit significant potential for application in cancer therapies in the future.

Data Availability

The data used to support the findings of this study are included within the article.

Conflicts of Interest

The authors declare no competing financial interest.

Authors' Contributions

Sanghyo Park and Hyungkyu Park contributed equally to this work.

Acknowledgments

This work was supported by the National Research Foundation of Korea (NRF) grant funded by the Korean Government (MSIP) (Nos. 2018R1D1A1B07042339 and 2015R1A2A2A07027863).

Supplementary Materials

Supplemental Figure 1: cytotoxicity of HA-MSNs against SCC7 cells. Supplemental Figure 2: cellular uptake of HA-Cy5.5-MSNs in SCC7 cells. Supplemental Figure 3: intracellular uptakes of DOX/HA-MSNs localized in nucleus that is observed with DAPI staining in blue. Supplemental Figure 4: intracellular Uptakes of Ce6/HA-MSNs. *(Supplementary Materials)*

References

[1] K. Park, *ACS Nano*, vol. 7, no. 9, pp. 7442–7447, 2013.

[2] G. Chen, H. Qiu, P. N. Prasad, and X. Chen, "Upconversion nanoparticles: design, nanochemistry, and applications in theranostics," *Chemical Reviews*, vol. 114, no. 10, pp. 5161–5214, 2014.

[3] E. C. Wang and A. Z. Wang, "Nanoparticles and their applications in cell and molecular biology," *Integrative Biology*, vol. 6, no. 1, pp. 9–26, 2014.

[4] H. Maeda, J. Wu, T. Sawa, Y. Matsumura, and K. Hori, "Tumor vascular permeability and the EPR effect in macromolecular therapeutics: a review," *Journal of Controlled Release*, vol. 65, no. 1-2, pp. 271–284, 2000.

[5] R. A. Petros and J. M. DeSimone, "Strategies in the design of nanoparticles for therapeutic applications," *Nature Reviews Drug Discovery*, vol. 9, no. 8, pp. 615–627, 2010.

[6] L. Palanikumar, J. Kim, J. Y. Oh et al., "Hyaluronic acid-modified polymeric gatekeepers on biodegradable mesoporous silica nanoparticles for targeted cancer therapy," *ACS Biomaterials Science & Engineering*, vol. 4, pp. 1716–1722, 2018.

[7] M. Gary-Bobo, D. Brevet, N. Benkirane-Jessel et al., "Hyaluronic acid-functionalized mesoporous silica nanoparticles for efficient photodynamic therapy of cancer cells," *Photodiagnosis and Photodynamic Therapy*, vol. 9, no. 3, pp. 256–260, 2012.

[8] J. Rosenholm, C. Sahlgren, and M. Linden, "Cancer-cell targeting and cell-specific delivery by mesoporous silica nanoparticles," *Journal of Materials Chemistry*, vol. 20, no. 14, pp. 2707–2713, 2010.

[9] D. Bechet, P. Couleaud, C. Frochot, M. L. Viriot, F. Guillemin, and M. Barberi-Heyob, "Nanoparticles as vehicles for delivery of photodynamic therapy agents," *Trends in Biotechnology*, vol. 26, no. 11, pp. 612–621, 2008.

[10] D. Tarn, C. E. Ashley, M. Xue, E. C. Carnes, J. I. Zink, and C. J. Brinker, "Mesoporous silica nanoparticle nanocarriers: biofunctionality and biocompatibility," *Accounts of Chemical Research*, vol. 46, no. 3, pp. 792–801, 2012.

[11] M. Vallet-Regí, "Mesoporous silica nanoparticles: their projection in nanomedicine," *ISRN Materials Science*, vol. 2012, Article ID 608548, 20 pages, 2012.

[12] K. Y. Choi, H. Chung, K. H. Min et al., "Self-assembled hyaluronic acid nanoparticles for active tumor targeting," *Biomaterials*, vol. 31, no. 1, pp. 106–114, 2010.

[13] J. Vivero-Escoto and M. Elnagheeb, "Mesoporous silica nanoparticles loaded with cisplatin and phthalocyanine for combination chemotherapy and photodynamic therapy in vitro," *Nanomaterials*, vol. 5, no. 4, pp. 2302–2316, 2015.

[14] A. M. Bugaj, "Targeted photodynamic therapy – a promising strategy of tumor treatment," *Photochemical and Photobiological Sciences*, vol. 10, no. 7, pp. 1097–1109, 2011.

[15] H. J. Cho, H. Y. Yoon, H. Koo et al., "Hyaluronic acid-ceramide-based optical/MR dual imaging nanoprobe for cancer diagnosis," *Journal of Controlled Release*, vol. 162, no. 1, pp. 111–118, 2012.

[16] F. Li, B. C. Bae, and K. Na, "Acetylated hyaluronic acid/-photosensitizer conjugate for the preparation of nanogels with controllable phototoxicity: synthesis, characterization, autophotoquenching properties, andin vitrophototoxicity against hela cells," *Bioconjugate Chemistry*, vol. 21, no. 7, pp. 1312–1320, 2010.

[17] H. Y. Yoon, H. Koo, K. Y. Choi et al., "Tumor-targeting hyaluronic acid nanoparticles for photodynamic imaging and therapy," *Biomaterials*, vol. 33, no. 15, pp. 3980–3989, 2012.

[18] T. A. Yap, A. Omlin, and J. S. de Bono, "Development of therapeutic combinations targeting major cancer signaling pathways," *Journal of Clinical Oncology*, vol. 31, no. 12, pp. 1592–1605, 2013.

[19] K. S. Albain, S. M. Nag, G. Calderillo-Ruiz et al., "Gemcitabine plus paclitaxel versus paclitaxel monotherapy in patients with metastatic breast cancer and prior anthracycline treatment," *Journal of Clinical Oncology*, vol. 26, no. 24, pp. 3950–3957, 2008.

[20] R. B. Mokhtari, S. Kumar, S. S. Islam et al., "Combination of carbonic anhydrase inhibitor, acetazolamide, and sulforaphane, reduces the viability and growth of bronchial carcinoid cell lines," *BMC Cancer*, vol. 13, no. 1, p. 378, 2013.

[21] S. Shen, M. Liu, T. Li, S. Lin, and R. Mo, "Recent progress in nanomedicine-based combination cancer therapy using a site-specific co-delivery strategy," *Biomaterials Science*, vol. 5, no. 8, pp. 1367–1381, 2017.

[22] G. Batist, K. A. Gelmon, K. N. Chi et al., "Safety, pharmacokinetics, and efficacy of CPX-1 liposome injection in patients with advanced solid tumors," *Clinical Cancer Research*, vol. 15, no. 2, pp. 692–700, 2009.

[23] C. He, Z. Tang, H. Tian, and X. Chen, "Co-delivery of chemotherapeutics and proteins for synergistic therapy," *Advanced Drug Delivery Reviews*, vol. 98, pp. 64–76, 2016.

[24] Q. Hu, W. Sun, C. Wang, and Z. Gu, "Recent advances of cocktail chemotherapy by combination drug delivery systems," *Advanced Drug Delivery Reviews*, vol. 98, pp. 19–34, 2016.

[25] L. D. Mayer, T. O. Harasym, P. G. Tardi et al., "Ratiometric dosing of anticancer drug combinations: controlling drug ratios after systemic administration regulates therapeutic activity in tumor-bearing mice," *Molecular Cancer Therapeutics*, vol. 5, no. 7, pp. 1854–1863, 2006.

[26] L. B. Josefsen and R. W. Boyle, "Unique diagnostic and therapeutic roles of porphyrins and phthalocyanines in photodynamic therapy, imaging and theranostics," *Theranostics*, vol. 2, no. 9, pp. 916–966, 2012.

[27] M. Gao, F. Fan, D. Li et al., "Tumor acidity-activatable TAT targeted nanomedicine for enlarged fluorescence/magnetic resonance imaging-guided photodynamic therapy," *Biomaterials*, vol. 133, pp. 165–175, 2017.

[28] F. Li, C. Chen, X. Yang et al., "Acetal-linked hyperbranched polyphosphoester nanocarriers loaded with chlorin e6 for ph-activatable photodynamic therapy," *ACS Applied Materials & Interfaces*, vol. 10, no. 25, pp. 21198–21205, 2018.

[29] C. Y. Sun, Z. Cao, X. J. Zhang, R. Sun, C. S. Yu, and X. Yang, "Cascade-amplifying synergistic effects of chemo-photodynamic therapy using ROS-responsive polymeric nanocarriers," *Theranostics*, vol. 8, no. 11, pp. 2939–2953, 2018.

[30] X. Wang, F. Li, X. Yan et al., "Ambient aqueous synthesis of ultrasmall $Ni_{0.85}Se$ nanoparticles for noninvasive photoacoustic imaging and combined photothermal-chemotherapy of cancer," *ACS Applied Materials & Interfaces*, vol. 9, no. 48, pp. 41782–41793, 2017.

[31] X. Wang, Z. Miao, Y. Ma, H. Chen, H. Qian, and Z. Zha, "One-pot solution synthesis of shape-controlled copper selenide nanostructures and their potential applications in photocatalysis and photothermal therapy," *Nanoscale*, vol. 9, no. 38, pp. 14512–14519, 2017.

[32] S. Kim, T. Y. Ohulchanskyy, H. E. Pudavar, R. K. Pandey, and P. N. Prasad, "Organically modified silica nanoparticles co-encapsulating photosensitizing drug and aggregation-enhanced two-photon absorbing fluorescent dye aggregates for two-photon photodynamic therapy," *Journal of the American Chemical Society*, vol. 129, no. 9, pp. 2669–2675, 2007.

[33] C. Conte, F. Ungaro, G. Maglio et al., "Biodegradable core-shell nanoassemblies for the delivery of docetaxel and Zn(II)-phthalocyanine inspired by combination therapy for cancer," *Journal of Controlled Release*, vol. 167, no. 1, pp. 40–52, 2013.

[34] A. Khdair, di Chen, Y. Patil et al., "Nanoparticle-mediated combination chemotherapy and photodynamic therapy overcomes tumor drug resistance," *Journal of Controlled Release*, vol. 141, no. 2, pp. 137–144, 2010.

[35] A. Khdair, H. Handa, G. Mao, and J. Panyam, "Nanoparticle--mediated combination chemotherapy and photodynamic therapy overcomes tumor drug resistance *in vitro*," *European Journal of Pharmaceutics and Biopharmaceutics*, vol. 71, no. 2, pp. 214–222, 2009.

[36] G. S. Trindade, S. L. A. Farias, V. M. Rumjanek, and M. A. M. Capella, "Methylene blue reverts multidrug resistance: sensitivity of multidrug resistant cells to this dye and its photodynamic action," *Cancer Letters*, vol. 151, no. 2, pp. 161–167, 2000.

[37] I. Slowing, J. Viveroescoto, C. Wu, and V. Lin, "Mesoporous silica nanoparticles as controlled release drug delivery and gene transfection carriers," *Advanced Drug Delivery Reviews*, vol. 60, no. 11, pp. 1278–1288, 2008.

[38] H. D. M. Follmann, O. N. Oliveira, D. Lazarin-Bidóia et al., "Multifunctional hybrid aerogels: hyperbranched polymer-trapped mesoporous silica nanoparticles for sustained and prolonged drug release," *Nanoscale*, vol. 10, no. 4, pp. 1704–1715, 2018.

[39] X. Mei, D. Chen, N. Li et al., "Facile preparation of coating fluorescent hollow mesoporous silica nanoparticles with pH-sensitive amphiphilic diblock copolymer for controlled drug release and cell imaging," *Soft Matter*, vol. 8, no. 19, pp. 5309–5316, 2012.

[40] H. S. Park, C. W. Kim, H. J. Lee et al., *Nanotechnology*, vol. 21, no. 22, article 225101, 2010.

[41] M. Yu, S. Jambhrunkar, P. Thorn, J. Chen, W. Gu, and C. Yu, "Hyaluronic acid modified mesoporous silica nanoparticles for targeted drug delivery to CD44-overexpressing cancer cells," *Nanoscale*, vol. 5, no. 1, pp. 178–183, 2013.

[42] S. Al-Qadi, A. Grenha, and C. Remunan-Lopez, "Microspheres loaded with polysaccharide nanoparticles for pulmonary delivery: Preparation, structure and surface analysis," *Carbohydrate Polymers*, vol. 86, no. 1, pp. 25–34, 2011.

[43] R. Zhang, R. Xing, T. Jiao et al., "Carrier-free, chemophotodynamic dual nanodrugs via self-assembly for synergistic antitumor therapy," *ACS Applied Materials & Interfaces*, vol. 8, no. 21, pp. 13262–13269, 2016.

[44] A. Hakeem, F. Zahid, R. Duan et al., "Cellulose conjugated FITC-labelled mesoporous silica nanoparticles: intracellular accumulation and stimuli responsive doxorubicin release," *Nanoscale*, vol. 8, no. 9, pp. 5089–5097, 2016.

[45] Y. Duo, Y. Li, C. Chen et al., "DOX-loaded pH-sensitive mesoporous silica nanoparticles coated with PDA and PEG induce pro-death autophagy in breast cancer," *RSC Advances*, vol. 7, no. 63, pp. 39641–39650, 2017.

[46] K. E. Uhrich, S. M. Cannizzaro, R. S. Langer, and K. M. Shakesheff, "Polymeric systems for controlled drug release," *Chemical Reviews*, vol. 99, no. 11, pp. 3181–3198, 1999.

[47] C. Rota, C. F. Chignell, and R. P. Mason, "Evidence for free radical formation during the oxidation of $2'$-$7'$-dichlorofluorescin to the fluorescent dye $2'$-$7'$ – dichlorofluorescein by horseradish peroxidase:Possible implications for oxidative stress measurements," *Free Radical Biology and Medicine*, vol. 27, no. 7-8, pp. 873–881, 1999.

[48] Z. Zhu, Z. Tang, J. A. Phillips, R. Yang, H. Wang, and W. Tan, "Regulation of singlet oxygen generation using single-walled carbon nanotubes," *Journal of the American Chemical Society*, vol. 130, no. 33, pp. 10856-10857, 2008.

[49] N. Han, Q. Zhao, L. Wan et al., "Hybrid lipid-capped mesoporous silica for stimuli-responsive drug release and overcoming multidrug resistance," *ACS Applied Materials & Interfaces*, vol. 7, no. 5, pp. 3342–3351, 2015.

[50] G. Capranico, K. W. Kohn, and Y. Pommier, "Local sequence requirements for DNA cleavage by mammalian topoisomerase II in the presence of doxorubicin," *Nucleic Acids Research*, vol. 18, no. 22, pp. 6611–6619, 1990.

[51] L. Wan, J. Jiao, Y. Cui et al., "Hyaluronic acid modified mesoporous carbon nanoparticles for targeted drug delivery to CD44-overexpressing cancer cells," *Nanotechnology*, vol. 27, no. 13, article 135102, 2016.